Egocentric Path Integration Models and their Application to Desert Arthropods

November 2, 2018

Tobias Merkle, Martin Rost and Wolfgang Alt

Theoretical Biology,
Mathematical and Natural Science Faculty,
University of Bonn
Kirschallee 1, D-53115 Bonn, Germany

Abstract

Path integration enables desert arthropods to find back to their nest on the shortest track from any position. To perform path integration successfully, speeds and turning angles along the preceding outbound path have to be measured continuously and combined to determine an internal *global vector* leading back home at any time. A number of experiments have given an idea how arthropods might use allothetic or idiothetic signals to perceive their orientation and moving speed. We systematically review the four possible model descriptions of mathematically precise path integration, whereby we favour and elaborate the hitherto not used variant of egocentric cartesian coordinates. Its simple and intuitive structure is demonstrated in comparison to the other models. Measuring two speeds, the forward moving speed and the angular turning rate, and implementing them into a linear system of differential equations provides the necessary information during outbound route, reorientation process and return path. In addition, we propose several possible types of systematic errors that can cause deviations from the correct homeward course. Deviations have been observed for several species of desert arthropods in different experiments, but their origin is still under debate. Using our egocentric path integration model we propose simple error indices depending on path geometry that will allow future experiments to rule out or corroborate certain error types.

Key words: Path integration, desert arthropod, egocentric, cartesian coordinates

1 Introduction

1.1 Path integration

Desert arthropods display the ability to return from a foraging excursion back to the nest on a straight way, often called the *home vector*. This ability to make a bee-line to the nest (or another location, such as a feeding site) without orientation on visible markers is based on an internal mechanism of *path integration* or *dead reckoning*, i.e. an integration of walking speed and angular variation along the arthropod's walking route. The result is a *global vector* that enables the arthropod to determine distance and direction of its nest at any position and time. After detecting and loading up the food, the arthropod just unreels that vector and, therefore, stays on the right and shortest track to its nest. Charles Darwin was the first to assume that animals may navigate this way (Darwin, 1873). About a century later first detailed investigations concerning arthropods (Jander, 1957; Görner, 1958, 1966; Wehner, 1968; Jander, 1970) were conducted. During the last 30 years, the general interest has focused more and more on the return path to the nest after foraging, and many investigations on both arthropods (e.g. Wehner and Wehner, 1986; Müller and Wehner, 1988; Bisch, 1999; Collett et al., 1999) and mammals (e.g. Mittelstaedt and Mittelstaedt, 1980; Séguinot et al., 1993; Benhamou, 1996, 1997; Séguinot et al., 1998) have been performed.

Apart from path integration, it has been shown that many species are capable of using landmarks to get their bearings (Hoffmann, 1985a; Collett et al., 1998; Bisch-Knaden and Wehner, 2003; Wehner, 2003). These landmarks, often referred to as *local vectors*, even seem to be preferred to the global vectors (Wehner et al., 1996; Collett et al., 1998) as navigational tool. However, before these vectors can be applied successfully, some information about their position has to be stored by the arthropod. Moreover, orientation with the aid of local vectors is error-prone, since landmarks can disappear or change their appearance, and, of course, is out of question for nests with no visible landmarks nearby.

The global vector gets updated on the complete trip, even if the orientation is conducted by using landmarks (e.g. Wehner et al., 1996; Collett et al., 1998, 2003). Moreover, it has been demonstrated that, after a sudden failure of the stored landmarks, desert ants *Cataglyphis fortis* revert to their global vector for orientation. Even if not used for several days, desert ants keep the global vector stored in their memory (Ziegler and Wehner, 1997). Thus, the relevance of global vectors as the main toolkit for homing seems to be as clear as the evolutionary necessity to develop abilities to measure the angular and linear components of the movements and to integrate them for having a home vector available whensoever.

A number of models (Jander, 1957; Mittelstaedt and Mittelstaedt, 1973; Müller and Wehner, 1988; Benhamou et al., 1990; Gallistel, 1990) try to point out mechanisms of path integration (for reviews, see Benhamou and Séguinot, 1995; Maurer and Séguinot, 1995; Biegler, 2000). Whereas earlier models use *geocentric* coordinates to represent the current global vector and the anticipated home direction, the more recent models are based upon the assumption

that internal calculation of the global vector, pointing from the animal's head to an anticipated nest position, should be performed in an *egocentric* coordinate system. In this case, however, mathematical computations and error estimations have so far been carried out only in *polar coordinates*, describing the distance and direction towards the nest with respect to the animals current position and walking direction.

Here we introduce a consistent model for *egocentric* path integration using *cartesian coordinates*. The mathematical computation of current nest position relative to the moving arthropod reduces to an inhomogeneous linear differential equation system of two variables, namely *forward moving speed* and *angular turning rate*. Different ways of their estimation and further processing implemented into this model provide several possibilities to reproduce some observed reorientation phenomena of arthropods.

The article is organised as follows. We finish the introductory Section reviewing more details on signal and information processing in homing arthropods. The next Section 2 is devoted to previous models of path integration. Section 3 presents our model approach and compares it to those in the previous Section. In Section 4 we turn to systematic errors in homing paths which have been studied extensively and may give hints about internal information processing. Taking advantage of the simple structure of our model we propose error tests for future experiments. Finally we discuss our results and briefly comment on possible neural realizations of egocentric cartesian path integration and possible generalisations including global vectors for feeding sites.

1.2 Required information for path integration

Allothetic and idiothetic signals provide the arthropod with the information required for path integration. During the following description of these signals, we shall focus on desert arthropods and here, in particular, on desert ants *Cataglyphis fortis* and *Cataglyphis bicolor*, because more is known on them as compared to other arthropods. Nevertheless, we shall also mention similar investigations on other arthropods in order to firmly base the modelling principles, mainly because neurobiological analyses have been performed on larger and more easily accessible arthropods (Wehner, 2003).

1.2.1 Allothetic signals

Without doubt, the main allothetic signals to be considered are visual inputs. Among them are landmarks which, however, have limited overall value as described above. More reliable turn out to be optical sources indefinitely far away: with regard to desert ants, spectral skylight gradient, sun position, and the pattern of polarised skylight are the most important cues (Wehner, 1997a,b, 2001, 2003; Wehner and Srinivasan, 2003). These three can work without help of each other, as was shown in experiments where one or even two of them had been made inoperative (Müller and Wehner, 1988; Wehner, 1997a). In all three the ants continuously use the sky as a reference to determine their body axis orientation.

Whenever the arthropod applies *spectral cues*, it makes use of the fact

that light waves with their different wavelengths are not equally distributed over the illuminated sky. This ability was shown by Wehner (1997a) for ants and Rossell and Wehner (1984) for bees.

Direct orientation with respect to the *azimuthal position* of the sun (or any other light source) has been found in ants and many other arthropods (e.g. bees, von Frisch, 1950; or spiders, Görner, 1958).

The *skylight polarisation* pattern, also referred to as skylight compass, represents the most effective and stable means for orientation in desert ants. Desert ants are able to see the e–vector polarisation pattern that is produced by scattering of the sunlight at air molecules in the atmosphere. This ability has been found in other arthropods and vertebrates as well, first of all in bees (von Frisch, 1949), but also, for instance, in desert locusts *Schistocerca gregaria* (Eggers and Gewecke, 1993), desert isopods *Hemilepistus reaumuri* (Hoffmann, 1984) or desert beetles *Parastizopus armaticeps* (Bisch, 1999). A small visible section of the sky has been shown to be sufficient to detect rotations (Fent, 1986; Wehner, 1994, 1997b).

Each rotation of the ant's body axis results in a corresponding change of this orientational angle allowing the ant to measure not only its current body direction relative to the allothetic skylight pattern, but also the rate of its angular rotation, independent of whether it is moving or turning on spot.

Although the polarised light pattern is changing with elevation of the sun, desert ants are able to use a stereotypical projection that resembles the skylight pattern at dawn or dusk, respectively, in their memory (Wehner, 1997a,b, 1998, 2001). Unlike for the task to find a feeder at different daytimes (Wehner, 1987; Wehner and Müller, 1993; Dyer and Dickinson, 1994) sun movement need not be compensated to find back during an excursion, which normally lasts only a few minutes, so the resulting error is negligible.

Although Ronacher and Wehner (1995) have shown that frontal optic flow influences the ants' odometer, the mechanisms to use allothetic cues for detecting *directions* and *rotations* seem to be inappropriate for measuring *distances* or *speeds*. Therefore, additional tools making use of idiothetic signals are needed.

1.2.2 Idiothetic signals

Far less is known about the use of idiothetic signals for the orientation of desert arthropods. Compared to allothetic signals they seem to be of minor or no importance for detecting directions. Experiments with desert ants have shown that it is possible to predict navigational errors by manipulating the visible section of the sky (Wehner, 1997a,b, 1998, 2001). Hence, the ants obviously do not even revert to proprioceptive signals if the polarisation compass as standard tool provides strange results. Also desert beetles *Parastizopus armaticeps* rely on the position of the light source and the polarisation compass and seem not to revert to proprioceptive cues in the case of ambiguities (Bisch, 1999). Desert ants *Cataglyphis fortis*, when captured at a feeder and transferred to a test area in a dark flask without any allothetic signals available, immediately after their release do reorientate and set out into their stored home direction (T. Merkle, personal observation). Thus, any possibly existing idiothetic signals do not have an effect on the

ant's reorientation under such conditions.

On the other hand, Ronacher and Wehner (1995) found that desert ants are able to estimate their walked distances without allothetic signals. Therefore they proposed that ants use odometers that mainly rely on proprioceptive signals. This is backed by investigations that could eliminate energy consumption as possible cue for measuring speeds or walking distances, when ants walk along slopes (Wohlgemuth et al., 2002) or with heavy load (Schäfer and Wehner, 1993). It seems quite obvious that such proprioceptive signals derive from movements of the legs (for bristles as mechanoreceptors cf. Keil, 1997).

2 Previous models of path integration

2.1 Geocentric models

The term path integration was established by Mittelstaedt and Mittelstaedt (1973), referring to a simple and evident mathematical algorithm, namely to determine the ant's current position by integrating its moving direction $\boldsymbol{\theta}(s)$ along the migration path or, equivalently, by integrating its velocity vector $\boldsymbol{V}(t) = v(t)\ \boldsymbol{\theta}(t)$ over time t, where $v(t)$ denotes the ant's forward speed. This yields the estimated final positional vector $\boldsymbol{P}$ from start to end point of the path. The estimated global *home vector* is then the inverse vector $\boldsymbol{G} = -\boldsymbol{P}$.

2.1.1 Cartesian coordinates

Mittelstaedt and Mittelstaedt (1973, 1982) use *cartesian coordinates* to represent the integrated positional vector $\boldsymbol{P} = (x, y)$ and the current directional vector $\boldsymbol{\theta} = (\cos\phi, \sin\phi)$, where the animal's angular orientation ϕ is given relative to some reference direction, e.g. skylight polarisation. This is chosen as the initial moving direction of the arthropod in their case study of the spider *Agelena labyrinthica*. In their model the arthropod is supposed to estimate the current angle ϕ in two different ways: by using an *idiothetic azimuth storage* as integrated value of its proprioceptively measured turning rates $\omega(t)$ along the previous path (this idea of azimuth integration is related to the earlier theory by Jander, 1957), or by directly measuring the *allothetic azimuth value* ϕ of the current body axis with respect to an exogenous direction. Then, the resulting two inputs of the directional vector $\boldsymbol{\theta}$ are weighted and summed up for path integration. With the aid of this model the authors could reproduce typical two–segment experiments, during which a light source had been turned by 90°.

It should be noticed that the described model of Mittelstaedt and Mittelstaedt (1973) is a closed-loop control system (*"Wirkungsgefüge"*) applicable to any excursion of an arthropod, including the outbound route towards a food source position $\boldsymbol{P}_0$, whose cartesian coordinates have to be internally stored, or the homing route towards the origin $\boldsymbol{P}_0 = (0, 0)$. In both cases the control system produces an efferent motor signal for the turning angle ω being negatively proportional to $|\boldsymbol{P}_0 - \boldsymbol{P}| \sin\delta$, where δ is the deviation angle between current moving direction ϕ and the global vector $\boldsymbol{G} = \boldsymbol{P}_0 - \boldsymbol{P}$. By this

steering algorithm, the arthropod will turn into the direction of the global vector and walk towards $\boldsymbol{P}_0$ until the global vector is zero. Thus, the path integration mechanism is supposed to work during the whole excursion.

This comprehensive navigation model has been adapted to experiments with rodents (e.g. Mittelstaedt and Mittelstaedt, 1980; Benhamou, 1997) or humans (Mittelstaedt and Mittelstaedt, 2001) and recently up–dated to be consistent with results on neural activity patterns in the hippocampus of mammals (Mittelstaedt, 2000). It provides important principles of information processing, path integration, and motor control, and is mathematically easily realizable in computer simulation programs. Nevertheless, it remains open, whether and how the necessary computational steps of calculating trigonometric functions are physiologically performed within the neural nets of arthropods or mammals. Moreover, this model supposes two successive integrating mechanisms including the necessity to store the computed variables, first $\phi = \int \omega \, dt$ and then $\boldsymbol{P} = \int (\cos\phi, \sin\phi) \, ds$, if integration is over walked distance, s denoting arc length, or, $\boldsymbol{P} = \int (v\boldsymbol{\theta})(t) \, dt$, if integration is over time. In the last case, besides determination of the turning speed ω, also that of forward speed v is required (see Table 1).

The extensive work on neural "head cell" and "place cell" dynamics in mammals could be mentioned here, with the remarkable property that a change in angular information, represented by head cells, can induce a corresponding rotation of the two–dimensional activity pattern in the imaginary chart represented by the array of place cells (Samsonovich and McNaughton, 1997; Mittelstaedt, 2000). With regard to *desert ants*, Wehner (2003) postulates the existence of a certain number of "compass neurons", each with an accurately defined compass direction resulting in a maximum firing rate of the respective neuron, whenever the arthropod is heading into that direction.

2.1.2 Polar coordinates

Geocentric models in *polar coordinates* have been developed and applied during the last 20 years by Wehner and Wehner (1986) and Müller and Wehner (1988), taken up by Hartmann and Wehner (1995) in connection with dynamical representations by cyclical neural chains. In order to represent the actual position vector $\boldsymbol{P} = r\,(\cos\nu, \sin\nu)$ of the arthropod, the proposed model algorithms require the animal to compute, at least approximately, distance r from the nest and angle ν of the position vector relative to an allothetic reference direction, determined by the sun or, most frequently, by polarised skylight. Then, the global home vector is $\boldsymbol{G} = -\boldsymbol{P} = r\,(\cos(\nu+\pi), \sin(\nu+\pi))$.

For a segmented path with step length s_n (taken to be 1 for simplicity), Müller and Wehner (1988) derive approximate recursive formulas for updating the polar coordinates (r_n, ν_n) after the nth moving step. The only additional input needed during each step, besides knowing step length (or measuring forward speed), is the angle $\tilde{\delta}_n = \phi_n - \nu_n$ between moving direction ϕ_n and the direction ν_n of the positional vector. In a continuous description the corresponding general path integration formulas read $r = \int \cos(\phi-\nu) \, ds$ and $\nu = \int \sin(\phi-\nu)/r \, ds$ and are equivalent to a system of nonlinear ordinary

differential equations (see also Table 1)

$$\frac{dr}{dt} = v\ \cos(\phi - \nu) \quad (1)$$

$$\frac{d\nu}{dt} = \frac{v}{r}\ \sin(\phi - \nu). \quad (2)$$

Again, as in Section 2.1.1, this mathematical integration algorithm requires the ability to calculate the nonlinear trigonometric functions and, in addition, to perform the division by distance r. Müller and Wehner (1988) and Hartmann and Wehner (1995) suggested the trigonometric functions could be approximated by piecewise linear or polynomial functions. This led to a systematic misestimation of increments in both variables, r and ν, for moving directions not parallel or antiparallel to the position vector, i.e. for $\tilde{\delta} = \phi - \nu \neq \pm\pi$. Müller and Wehner (1988) thus could remarkably well reproduce systematic errors in the angular component ν of the global vector, observed in the classical two–segment experiments, not only for desert ants but also for most arthropods and mammals (e.g. Bisetzky, 1957; Görner, 1958; Müller and Wehner, 1988; Séguinot et al., 1993). In Section 4.3 we give a detailed analysis of this topic.

2.2 Egocentric models

Another approach, which appears to be more adequate but came into consideration much later, is to model the path integration process of a moving animal in terms of a moving coordinate frame centred around the animal's body, thus reflecting the fact that it perceives all sensory inputs relative to its own position and orientation. Benhamou et al. (1990) chose *polar coordinates* to represent the global vector $\boldsymbol{G} = -\boldsymbol{P} = r\,(\cos\delta, \sin\delta)$, where now the reference direction for $\delta = 0$ is the body axis, serving as X–axis of the corresponding cartesian coordinate frame with the orthogonal lateral Y–axis, see Fig. 1. Although the distance variable r is the same as in the geocentric polar model, the derived recurrent formulas for updating r_n and δ_n turn out to be much more complicated than any other formula used before. First, egocentric cartesian coordinates (X_n, Y_n) are updated in terms of the former polar ones,

$$X_{n+1} = r_n\ \cos(\delta_n - \omega_n) - s_n \quad (3)$$

$$Y_{n+1} = r_n\ \sin(\delta_n - \omega_n) \quad (4)$$

where ω_n denotes the change of the direction and s_n the length of the subsequent step. (An interchange of the order of stepping and turning would give s_{n+1} in (3) but no fundamental change). Then, these equations are transformed into the new egocentric polar coordinates:

$$r_{n+1} = \sqrt{{X_{n+1}}^2 + {Y_{n+1}}^2} \quad (5)$$

$$\delta_{n+1} = \arctan\left(\frac{Y_{n+1}}{X_{n+1}}\right) \quad (6)$$

(in order to calculate the correct values of δ_{n+1} the signs of X_{n+1} and Y_{n+1} have to be considered, see Benhamou and Séguinot, 1995).

The advantage of this egocentric model is that now the only *input variables* are step length s_n and turning angle ω_n, or, in the corresponding continuous path integration model, forward speed v and angular turning rate ω. Gallistel (1990) considered the corresponding differential equation using egocentric polar coordinates in the continuous limit of infinitely small time steps which, in the corrected formulation by Benhamou and Séguinot (1995), are

$$\frac{dr}{dt} = -v \cos\delta \tag{7}$$

$$\frac{d\delta}{dt} = v \frac{\sin\delta}{r} - \omega. \tag{8}$$

These equations can directly be obtained form the corresponding polar coordinate equations, Eqs. (1) and (2), by performing a simple angular transformation, $\delta = \nu + \pi - \phi$, so that again they require to compute division by r and trigonometric functions (see also Table 1).

In their simulation analysis, Benhamou et al. (1990) studied the influence of random errors on the estimation of changes of direction and walking distance. With regard to directional changes, they distinguished between allothetical and idiothetical orientation: they considered idiothetical estimation as "measuring the change of direction itself", whereas the allothetical estimation is defined as "a comparison between the heading of current and previous step relative to some exteroceptive compass" (Maurer and Séguinot, 1995). The different estimation procedures were realized by providing the actual values with normal distributed errors.

In their simulations random errors of allothetic signals had only little influence, whereas those of idiothetic signals lead to noticeable misestimation. Benhamou and Séguinot (1995) conclude that the egocentric coding process is quite sensitive to idiothetic errors and organisms relying on allothetic cues for measuring directional changes by far outmatch those relying on idiothetic cues.

3 Cartesian model for egocentric path integration

3.1 System of linear differential equations for the global vector

The physiological sensing and locomotion apparatus of any arthropod is completely bound to its body. It is therefore naturally related to its two symmetry axes, the posterior-anterior axis and the perpendicular right-left axis. Thus, when identifying these symmetry axes with the X and Y axis of a cartesian coordinate frame (X, Y) and taking the arthropod's body centre as the origin $(0, 0)$, this constitutes a proper planar moving coordinate frame for representing the *relative position* of any object in the planar neighbourhood of the arthropod, e.g. its nest. In this *egocentric cartesian* model the global vector pointing from the arthropod's body to the nest, relative to the animal's actual body axis orientation, is just $\boldsymbol{G} = (X, Y)$, corresponding to

the same vector as in Section 2.2, there only written in polar coordinates, see Fig. 1. Notice that the original ansatz by Benhamou et al. (1990) already mentioned this cartesian coordinate system, but then switched to polar coordinates for path integration (see Section 2.2). Indeed, the continuous version of Eqs. (3) and (4), given the arthropod's *forward speed* v and *angular turning rate* ω, yields the following model equations for a precise update of the global vector (X, Y) during motion

$$\frac{dX}{dt} = -v + \omega \cdot Y \tag{9}$$

$$\frac{dY}{dt} = -\omega \cdot X \tag{10}$$

Compared to all other continuum equations or analogous discrete recursion algorithms developed previously (see Section 2), this two–dimensional differential equation system is remarkably simple: It is linear in the two variable quantities X and Y, and it just uses the two speed input parameters as additive or multiplicative terms, v representing the rate of shifting the X coordinate backwards, ω the rate of rotating the (X, Y) frame clockwise. These operations can be easily performed by any suitable elementary analogue circuit network like the one shown below in Fig. 3. Possible physiologically realizable neural representations are briefly addressed in the Discussion Section 5.

In conclusion, this *cartesian egocentric path integration model*, considered as a precise 'dead reckoning' system, offers the most simple computational scheme to determine the global vector and, simultaneously, being related to a coordinate frame of the moving arthropod. For comparison with the other models see Table 1.

Clearly, biological solutions of difficult problems can be complex and the simplicity of our model does not make its realisation more likely than that of other models. From a conceptional point of view the existence of a simple solution is nevertheless striking, and in the following we shall present its implementation and results.

		Input variables	Internal variables	Global vector
Geocentric	Cartesian *(Sect. 2.1.1)*	ω,v or ω_n,s_n	ϕ, $\boldsymbol{P} = (x, y)$ ⟨lin./nonlin. ODE⟩	$\boldsymbol{G} = \boldsymbol{P}_0 - \boldsymbol{P}$
	Polar *(Sect. 2.1.2)*	ϕ s_n or v	r and ν ⟨nonlinear ODE⟩	$\boldsymbol{G} = -r\ (\cos\nu, \sin\nu)$
Egocentric	Polar *(Sect. 2.2)*	ω,v or ω_n,s_n	r and δ ⟨nonlinear ODE⟩	$\boldsymbol{G} = r\ (\cos\delta, \sin\delta)$
	Cartesian *(Sect. 3)*		X and Y ⟨linear ODE⟩	$\boldsymbol{G} = (X, Y)$

Table 1: Path integration models with the parameters and variables used for input, internal calculation and output as global vector. For notations and more details see the various model descriptions in the text.

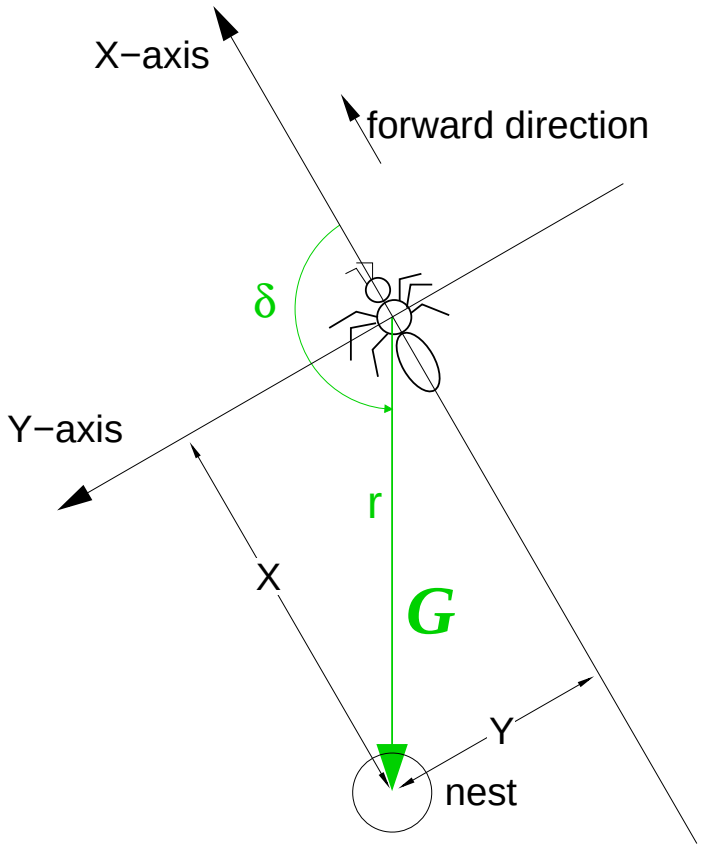

Figure 1: Theoretical scheme of egocentric path integration by means of cartesian coordinates X, Y specifying the position of the nest relative to the arthropod's body axes and determining the global vector $\boldsymbol{G} = (X, Y)$, here with $X < 0$, $Y > 0$. In contrast, the corresponding model in polar coordinates (Section 2.2) uses the two variables r, distance to the nest, and δ, angle between head orientation and nest direction.

3.2 Modelling foraging excursions, reorientation, and homing

Our path integration model depends on the values of v and ω, cf. Table 1. These can be regarded as the elementary physiological control variables which the arthropod uses to steer its locomotion, e.g. by changing speed or frequency of striking leg motion on both sides or, respectively, on one side relative to the other.

In order to model typical paths of directionally persistent random walks, as observed for desert arthropods, one has to account for mean values and standard deviations of speed v and turning rate ω as well as for their temporal auto-correlations which can be extracted from corresponding experimental time series (see Alt, 1990). Discrete correlated random walk models sometimes used (e.g. Byers, 2001) are not adequate as they assume piecewise constant walking directions ϕ_n and turning angles ω_n. The two speeds $v(t)$ and $\omega(t) = d\phi(t)/dt$, however, being related to the physiologically controlled,

relatively fast leg movement on both sides of the arthropod, should better be modelled as fluctuating continuous processes on an adequate smoothness level. The simplest stochastic process of this kind is described by the following two independent Ornstein–Uhlenbeck equations for first order coloured noise, which have previously been used also for modelling the systematic search of arthropods (Alt, 1995),

$$dv = \frac{1}{T_v}\,(v_0 - v)\,dt + \beta_v\,dW_t \tag{11}$$

$$d\omega = \frac{1}{T_\omega}\,(\omega_0 - \omega)\,dt + \beta_\omega\,dW_t \tag{12}$$

Following the standard approach, random perturbations are expressed as additive Wiener increments dW_t (Itô and McKean, 1965). In simulations one uses a sequence of values v and ω with *finite* time differences τ,

$$v_{t+\tau} = v_t + \frac{\tau}{T_v}\,(v_0 - v_t) + \beta_v\sqrt{\tau}\,\zeta \tag{13}$$

$$\omega_{t+\tau} = \omega_t + \frac{\tau}{T_\omega}\,(\omega_0 - \omega_t) + \beta_\omega\sqrt{\tau}\,\zeta \tag{14}$$

where ζ denotes a standard normally ($\mathcal{N}(0,1)$) distributed random variable, drawn independently at each step for each variable. Eqs. (11) and (12) are obtained in the limit $\tau \to 0$. v_0 and ω_0 are the preferred values of forward and turning speed, respectively, and the $T_{v|\omega}$ denote the corresponding mean persistence times of fluctuations with amplitudes $\beta_{v|\omega}$. In case of a stationary time series they yield variances of size $\sigma^2_{v|\omega} = \beta^2_{v|\omega}T_{v|\omega}/2$ by an equilibrium of perturbations with strength $\beta_{v|\omega}$ and decay at rate $1/T_{v|\omega}$. In our presentation we assume, for simplicity, that T_v is negligibly small, such that during locomotion the forward moving speed has a constant value $v \equiv v_0$. The presented results also hold for the general case of fluctuating forward speed.

In the following, we describe the three successive phases of an arthropod's typical excursion, using the egocentric path integration system Eqs. (9), (10) and the physiological motion control system Eqs. (11) and (12). We explain the corresponding dynamics of the global vector by means of a simulated example presented in Fig. 2.

- Phase 1: **(Foraging)**
  The arthropod starts foraging at the nest site, e.g. $(x_0, y_0) = (0, 0)$, where the global vector is reset to zero $\boldsymbol{G} = (X, Y) = 0$. Holding the mean turning rate $\omega_0 = 0$, the animal approximately keeps its chosen initial direction, $\phi = \phi_0$, for some time, leading it almost straight away from the nest, corresponding to increasingly negative X values of the internal global vector, while the Y component stay close to zero. This initial behaviour is well expressed in the example of Fig. 2, then followed by a random right-hand turn of the (x, y)-path, which corresponds to increasingly Y values meaning that now the nest lies to the right side the animal.

- Phase 2: **(Reorientation)**
  After finding food at some position $\boldsymbol{P}_1 = (x_1, y_1)$, the arthropod stops

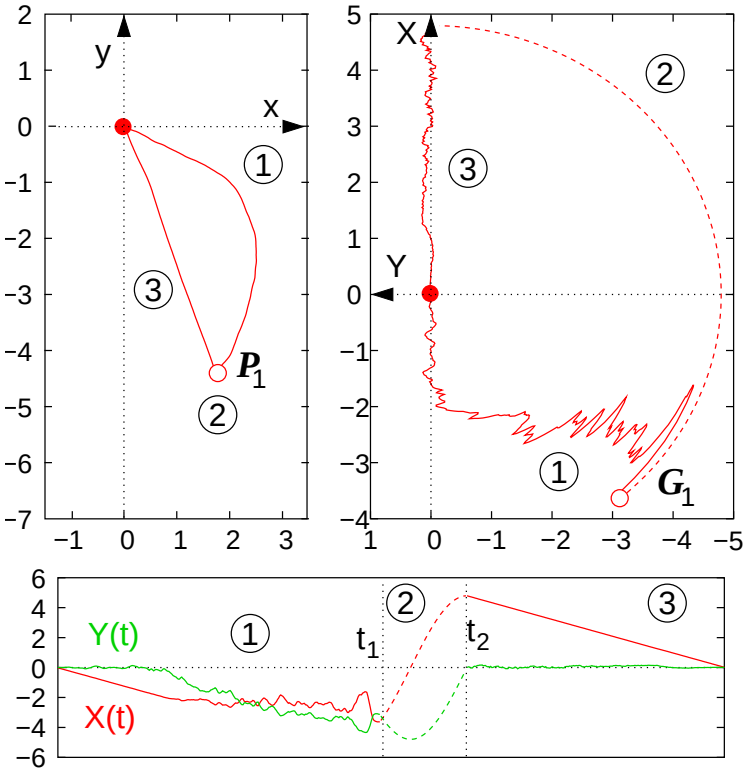

Figure 2: Model simulation of a natural outbound path and the successful return path back to the nest due to precise path integration, according to the 3-Phase-model, see text. Parameters used for calculations are, (1) for the outbound path $T_\omega = 0.3$ s, $\beta_\omega = 1$ s$^{-3/2}$, and constant forward speed $v \equiv v_0 = 0.2$ m/s, (2) constant $\omega_{\rm rot} = 1$ s^{-1} during rotation and (3) for homing the same as in (1) but a feedback constant $c = 1/0.05$ s^{-1} for beacon steering. (Top left): Plot of the actual path in cartesian (x, y)-coordinates of an observer. Position of the nest at $(0, 0)$ is marked by a filled circle. (Top right): Corresponding plot of the nest position in the same scale in relative cartesian (X, Y)-coordinates, where the origin denoting the home position is marked by a filled circle. Note that the animal's head direction is the X–axis pointing upwards, while the lateral Y–axis points to the left. (Bottom): Corresponding plots of X and Y over time.

there in its current angular orientation, $\phi = \phi_1$, keeping the actual global vector $\boldsymbol{G}_1 = (X_1, Y_1)$ internally stored (even during handling the food). Then the arthropod starts its reorientation phase by turning on spot, say with constant rotation speed $\omega \equiv \pm\omega_{\rm rot}$, depending on whether the stored global vector $\boldsymbol{G}_1$ has positive or negative Y_1 value. During rotation the global vector $\boldsymbol{G} = (X, Y)$ also rotates according to path integration in Eqs. (9) and (10), since now we set $v \equiv v_0 = 0$. Finally, the arthropod is assumed to stop its rotation ($\omega = 0$) as soon as the condition $Y = 0$ is fulfilled, meaning that now its head is oriented towards the nest and the actually positive X-value represents the arthropod's distance from the nest (cf. the scheme in Fig. 3). For the example in Fig. 2, see the counter-clockwise rotation circle ending

on the positive X axis. Notice that the condition $Y = 0$ corresponds to $\delta = 0$ in egocentric polar coordinates (Section 2.2 and Fig. 1) because of the equivalences $Y = r \cdot \sin\delta$ ($\approx r\delta$ for small δ) and $X = r \cdot \cos\delta$ ($\approx r + r\delta^2/2$ for small δ).

- Phase 3: **(Homing)**
  The arthropod now returns back to the nest (as straight as possible) according to the actually stored global vector $\boldsymbol{G} = (X, 0)$. Since during walking the global vector will be constantly updated and, due to inevitable random perturbations, the Y component will eventually deviate from the zero value, the arthropod must tend to hold the internal *steering condition* $Y = 0$ as closely as possible. This can be modelled by implementing a *counter-steering* turning rate $\omega_0 = -cY$ into the stochastic differential equation (12). See Fig. 3 for an analogue circuit scheme describing this feedback control, which nonlinearly and cyclically couples the linear path integration system, Eq. (9) and (10), to the linear motor control equation (12).

  Finally, in our model the arthropod is assumed to stop its return phase as soon as the X value of its global vector becomes zero. The resulting home path in the simulated example of Fig. 2 clearly shows, how some random perturbations lead to small deviations in the homing direction of the (x, y) path and corresponding small Y deviations of the global vector, while the X component is almost linearly decreasing to zero.

Notice that, according to this modelling scheme, the path integration system in Eqs. (9) and (10) is supposed to work constantly in the arthropod's neural system during foraging, reorienting, and homing, except when the animal is seriously perturbed and not any more able to 'measure' and 'control' its forward motion and directional turning. If this happens, the animal is assumed to instantaneously halt the path integration system and keep the actual value of the egocentric global vector and the orientational angle (with respect to an allothetic visual cue) stored until it can proceed in an unperturbed way.

Let us emphasise, that the presented *internal* dynamics of the global vector $\boldsymbol{G} = (X, Y)$ determined by the simple linear system differential equations (9) and (10), could equivalently be described in polar coordinates $\boldsymbol{G} = r\,(\cos\delta, \sin\delta)$ using the more complicated nonlinear differential equations (7) and (8), including the 'rotation stop condition' $\delta = 0$ and the counter-steering term $\omega_0 = -c\,r\cos\delta$ or a stronger variant like $\omega_0 = -\tilde{c}\,\delta$. However, there is an important difference in modelling the 'nest stop condition': In polar coordinates, the obvious termination criterion would be chosen as $r = 0$ meaning that the global vector $\boldsymbol{G}$ becomes exactly zero. It remains to be proven, which counter-steering rule could guarantee that this condition is attainable for stochastically perturbed random paths.

In contrast, the proposed termination criterion $X = 0$ in cartesian coordinates would, for randomly perturbed return paths, generically result in a non-vanishing small Y value, then representing the lateral distance of the arthropod to the nest. Thus, depending on this value and on the current orientational angle of the animal, the realized 'stop position' can fluctuate

around the true nest position, even in the so far considered case of *precise path integration*. The size of this random error increases with the length of the home vector, i.e. the distance between food and nest. This corresponds to experimental observations (e.g. for desert ants *C. fortis* T. Merkle, unpublished data) which furthermore show that the length of the outbound path also contributes to such a positional error. Therefore, other errors in path integration, being accumulated along the path, have also to be considered, which is the topic of the following Section.

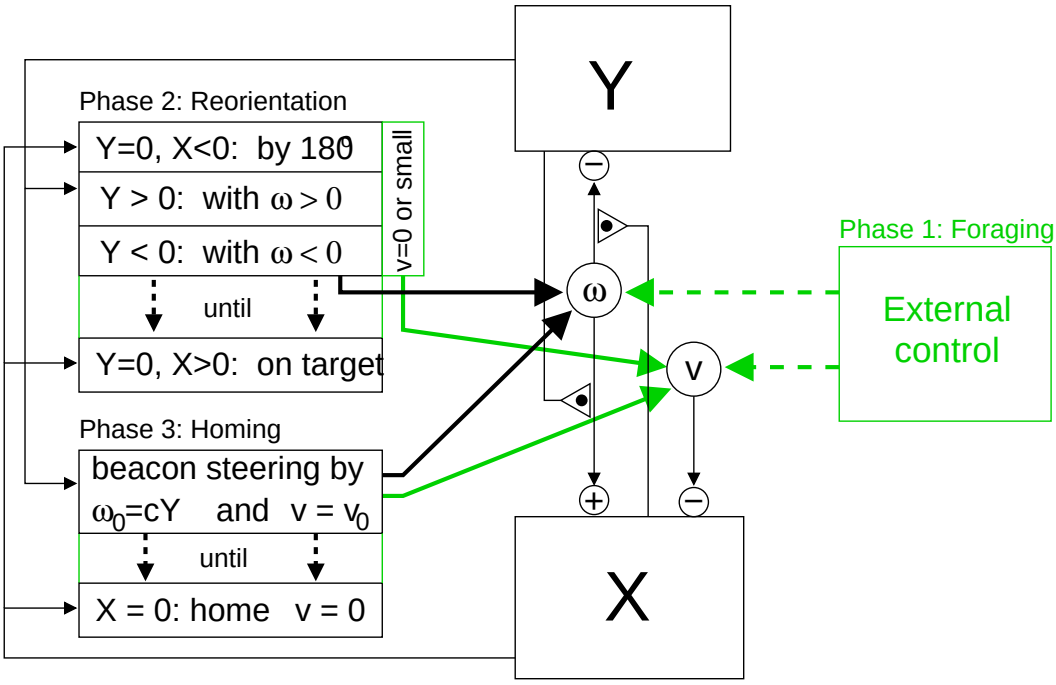

Figure 3: Analogue circuit scheme of the egocentric cartesian path integration model: dynamics of the two variables X and Y according to the differential equations (9) and (10) and its coupling to the physiological control parameters represented by the two speed parameters for turning, ω, and forward locomotion, v. In **Phase 1**, ω and v are externally controlled (random search, trained path towards feeder, ...). During **Phase 2** and **Phase 3** the X and Y values feed back into the speed control conditions such that, by counter–steering with respect to the 'internal beacon' $Y = 0$ in the latter case, equations (9), (10) and (12) constitute a coupled nonlinear control system along the homing path.

4 Systematic errors

It has been shown that many arthropods (e.g. Bisetzky, 1957; Görner, 1958; Hoffmann, 1985b; Wehner and Wehner, 1986; Müller and Wehner, 1988) but also mammals (e.g. Séguinot et al., 1993; Etienne et al., 1996; Séguinot et al., 1998) exhibit errors in determining the exact homing direction. In general, we have to distinguish between random errors and systematic errors during path integration. There is evidence that random errors, in addi-

tion to the home vector steering error mentioned above, can originate from inaccurate measurements of angles or distances, whereas systematic errors probably arise at the neural level of the organism (Benhamou et al., 1990; Séguinot et al., 1998). Orientation is less error prone if allothetic reference frames are available, as polarised skylight for arthropods (e.g. Wehner, 1998, 2003), but a more difficult task if not, as for mammals (Etienne and Jeffry, 2004). Systematic errors play an important role, as the classical two–leg experiments (L-shaped angular turning tests) have shown in both mammals (e.g. Maurer and Séguinot, 1995; Etienne et al., 1996) and arthropods (e.g. Müller and Wehner, 1988; Bisch, 1999). Apart from mistakes that concern directional aberrations, there occur also errors by underestimation of distances (Sommer and Wehner, 2004).

From an evolutionary point of view the presence of systematic homing errors is interesting and has not been explained to date. It may have an advantage that a homing animal typically assumes a shorter path and ends up *in front of* its nest. It would then avoid an overshoot and find familiar features that it has just passed on the outgoing path which might help to reach the nest's entrance.

In this Section we implement two types of systematic errors into our model. One concerns the estimation of nest distance following Sommer and Wehner (2004), the other exhibit different variations in processing the turns during path integration. All of them predict systematic deviations from correct homeward courses and are based on feasible neural assumptions, or reproduce behaviours that have been observed during experiments. They may serve as a basis for ongoing and future studies of systematic deviations (T. Merkle, unpublished data).

4.1 Underestimation of turning angles

Müller and Wehner (1988) trained desert ants to run through two channels of 10m and 5m length and varied the connecting angle between them in several steps from 0 to 180°, see Figs. 4 and 5. The ants miscalculated their covered outbound route and, after leaving the second channel's end, turned about an angle which was *larger* than the correct one leading home. The authors reproduced this error very well by a simple formula, which accumulates systematic miscalculations in path integration whenever the animal walks different from the direct inbound and outbound directions. In Fig. 5 the angular aberration function ε is shown, computed according to the approximative path integration model by Müller and Wehner (1988). In general, this function fits quite well observations in other arthropods and mammals (Séguinot et al., 1993; Bisch, 1999). Here we show that other error models can also reproduce these data. For evaluation and fitting of the corresponding error functions (see plots in Fig. 5) we use the advantages of our egocentric path integration system.

As a first error mechanism we consider a *systematic underestimation* of body axis rotation. In principle, that error could occur during the estimation of ω, i.e. by simply perceiving a value lower than the actual value, or on the neural level. The high accuracy concerning the ability of desert arthropods measuring rotations makes it very likely that this error may be created on

the neural level. Therefore, we assume the animal perceives the correct value ω_{real}, but uses a different value ω_{proc} for processing the path integration according to the differential equations (9) and (10).

In a first choice the underestimation is taken to be a linear function of the real value,

$$\omega_{\mathrm{proc}} = \lambda\, \omega_{\mathrm{real}} \tag{15}$$

with a factor $\lambda < 1$ (error LU in Table 2). In a second variant, the fully saturated underestimation, ω_{real} is processed correctly for small values but saturates towards a certain maximal turning rate ω_{c} (error NLUs in Table 2),

$$\omega_{\mathrm{proc}} = \frac{\omega_{\mathrm{c}}}{\omega_{\mathrm{c}} + |\omega_{\mathrm{real}}|}\, \omega_{\mathrm{real}} \tag{16}$$

A linear combination of both is given by the error NLU in Table 2,

$$\omega_{\mathrm{proc}} = \left(\lambda + \frac{1-\lambda}{\omega_{\mathrm{c}} + |\omega_{\mathrm{real}}|}\, \omega_{\mathrm{c}}\right)\, \omega_{\mathrm{real}} \tag{17}$$

which again processes small values correctly.

For a related choice of errors we assume a temporal delay τ_{del} in processing the information of $\omega_{\mathrm{real}}(t)$; the same underestimation could, in principle, be assumed also for $v_{\mathrm{real}}(t)$, but here variation on natural outbound paths is rather low (T. Merkle, personal observations on desert ants *Cataglyphis fortis*). Phenomenologically such a delay is implemented by a linear ordinary differential equation representing a first order filtering process, namely

$$\frac{d\omega_{\mathrm{proc}}}{dt} = \frac{\omega_{\mathrm{real}} - \omega_{\mathrm{proc}}}{\tau_{\mathrm{del}}} \tag{18}$$

such that ω_{proc} is *smeared out* on a scale of τ_{del} as compared to ω_{real} (error PD in Table 2).

4.2 Underestimation of distance to the nest

The error due to distance underestimation, which we consider here, has previously been referred to as *leaky integrator* by Sommer and Wehner (2004). This idea can be implemented into our egocentric cartesian path integration model in a straightforward way: with a constant rate the integrated global vector "leaks" or decays from the memory. Thus, the two–dimensional model Eqs. (9) and (10) are varied by simply adding a proportional decay term in each equation (error LI in Table 2)

$$\dot{X} = -v + \omega_{\mathrm{real}} Y - \frac{X}{\tau_{\mathrm{L}}} \tag{19}$$

$$\dot{Y} = -\omega_{\mathrm{real}} X - \frac{Y}{\tau_{\mathrm{L}}} \tag{20}$$

with mean decay time τ_{L}. Also in egocentric polar coordinates, c.f. Eqs. (7) and (8), the leaky integrator is easily expressed by a proportional decay of radial distance r, see Table 2.

In the case of a one–dimensional path, e.g. always walking along x without any turns ($\omega_{\rm real} \equiv 0$), Eqs. (19) and (20) lead to an exponential underestimation ($x_{\rm ue}$) of the actual walking distances (x) as

$$x_{\rm ue} = \xi_{\rm L} \left(1 - \exp(-x/\xi_{\rm L})\right). \tag{21}$$

The estimated distance $x_{\rm ue}$ saturates at a length $\xi_{\rm L} = v\tau_{\rm L}$ in the limit of long walking distances x, but for short paths $x \ll \xi_{\rm L}$ the error is small and $x \approx x_{\rm ue}$.

This is precisely the best fit to the experiments performed by Sommer and Wehner (2004). The authors trained desert ants to walk through linear channels to a feeder. Afterwards the ants were captured at the feeder and released in a linear test channel. They headed off in homeward direction and performed a back and forth search around their assumed nest position. By extracting $x_{\rm ue}$ from the search behaviour, Sommer and Wehner found the relation of Eq. (21).

In a truly two–dimensional path the leaky integrator of (19) and (20) may also lead to an *angular deviation* of the search path from the true homeward direction. Earlier sections of the outgoing path have decayed in the memory more than later ones. If the animal has turned in–between, this will result in a *different* misestimation of related directions and, consequently, in a homing angle misestimation. In Fig. 4 this is explained for the classical two–leg experiment of Müller and Wehner (1988).

There is, however, a quantitative mismatch between the fit of the LI equations (19) and (20) to the experiments of Müller and Wehner (1988) and to those of Sommer and Wehner (2004). In the latter case one obtains $\xi_{\rm L} \approx 90$m which is substantially different from the value of 18m of the fit to Müller's and Wehner's two–leg experiments. At present we conclude that most likely some part of the error occurs during the turn. To fully answer this contradiction, one would have to take into account more details of the ants' walks, such as, e.g., walking speed or waiting times.

Up to now we have proposed different elementary error mechanisms. Based on current knowledge of sensoric and neural processes it is not possible to prove or refuse their validity. They nevertheless lead to non–trivial consequences which are not immediately visible but can be seen in simulated realizations of outbound routes together with the path integration procedure.

4.3 Resulting deviations

First, we document the outcome of a simulated experiment as in Müller and Wehner (1988). The left side of Fig. 4 shows a sketch of the two–leg experimental setup which in Müller and Wehner (1988) had lengths $a = 10$m and $b = 5$m. The ant starts at the nest (open circle), turns after distance a by an angle $0 \le \alpha \le \pi$ to the right, leaves the channel after another walked distance b (at the black circle), thereby overcompensating its turn to the correct home direction by an angular deviation ε.

The right side of Fig. 4 represents this path in the internal (X, Y)–coordinates. First consider a correct processing without any systematic error: X decreases to $-a$ (thick black line) and $Y = 0$, then the animal turns by an angle α, such that now $X = -a\cos\alpha$ and $Y = -a\sin\alpha$ (black dashed line),

Error	Differential Equations
Turning rate underestimation	
LU linear underestimation of ω $\omega_{\text{proc}} = \lambda\,\omega_{\text{real}}, \quad 0 < \lambda < 1$	
NLUs fully saturated underestimation $\omega_{\text{proc}} = \frac{\omega_{\text{c}}\omega_{\text{real}}}{\omega_{\text{c}} + \lvert\omega_{\text{real}}\rvert}$ with $\omega_{\text{c}} > 0$	
NLU partially saturated underest. $\omega_{\text{proc}} = \omega_{\text{real}}\left(\lambda + \frac{1-\lambda}{\omega_{\text{c}} + \lvert\omega_{\text{real}}\rvert}\,\omega_{\text{c}}\right)$	$\dot{X} = -v + \omega_{\text{proc}}\,Y$ $\dot{Y} = -\omega_{\text{proc}}\,X$
PD processing delay $\dot{\omega}_{\text{proc}} = \frac{\omega_{\text{real}} - \omega_{\text{proc}}}{\tau_{\text{del}}}$	
Nest distance underestimation	
LI Leaky integrator	
egocentric cartesian	$\dot{X} = -v + \omega_{\text{real}}\,Y - X/\tau_{\text{L}}$ $\dot{Y} = -\omega_{\text{real}}\,X - Y/\tau_{\text{L}}$
egocentric polar	$\dot{r} = -v\cos\delta - r/\tau_{\text{L}}$ $\dot{\delta} = v\sin\delta/r - \omega_{\text{real}}$

Table 2: Error types in path integration and their respective formulae.

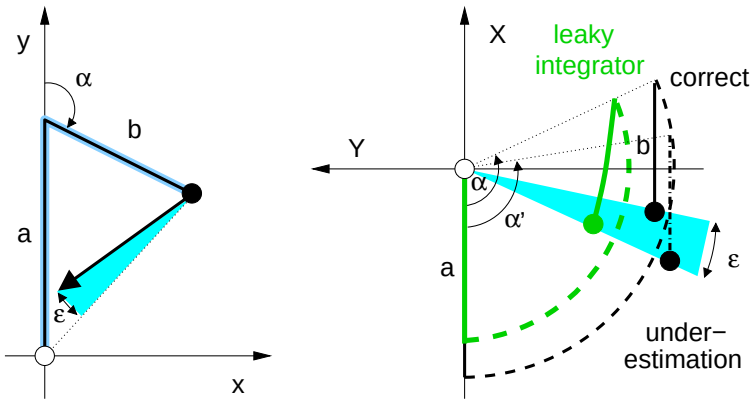

Figure 4: Angular deviation ε in the two–leg experiment with channels of length a and b, respectively, and clockwise connecting angle α. (Left side): Experimental situation as observed in geocentric (x, y)–coordinates. (Right side): Representation of the global vector in internal (X, Y)–coordinates; correct representation indicated by thick black line, dashed during counter-clockwise turn about angle α. *Angle underestimation* leads to turn by $\alpha' < \alpha$ and angular aberration ε after leaving the second channel (black dot–dashed line). *Leaky integrator* is shown in grey, also leading to angular deviation. For more details see text.

finally X decreases further to $X = -a\cos\alpha - b$, whereas Y remains constant (black solid line with black circle). *Angle underestimation* would result in a turn by $\alpha' < \alpha$ such that in the end $X = -a\cos\alpha' - b$ (dot–dashed line with

black circle) which lies off the true direction to the nest by an error angle ε. A similar result is obtained by the *leaky integrator* (fat grey lines): First X decreases from 0 to $-\xi_{\mathrm{L}}\,(1-\exp(-a/\xi_{\mathrm{L}}))$ and Y remains 0 (thick grey line), then X and Y are turned by an angle α (dashed grey line). The turn occurs so fast that "leakage" can be neglected ($\tau_{\mathrm{turn}} \approx r_{\mathrm{turn}}/v \ll \tau_{\mathrm{L}}$, see also below). During the final decrease of X, both the values of X and Y "leak" such that finally

$$X_{\mathrm{L}} = -\xi_{\mathrm{L}}\,\left[e^{-b/\xi_{\mathrm{L}}}\left(1-e^{-a/\xi_{\mathrm{L}}}\right)\cos\alpha + \left(1-e^{-b/\xi_{\mathrm{L}}}\right)\right] \quad (22)$$

$$Y_{\mathrm{L}} = -\xi_{\mathrm{L}}\,e^{-b/\xi_{\mathrm{L}}}\left(1-e^{-a/\xi_{\mathrm{L}}}\right)\sin\alpha \quad (23)$$

which is indicated by the filled grey circle, again resulting in an angular deviation ε (in the sketch, for simplicity, the same as for angle underestimation).

The three upper curves of Fig. 5 show theoretical predictions for the angle error ε in the two–leg experiment of Müller and Wehner: the error according to the formula of Müller and Wehner (1988) calculated numerically as a function of the angle $0 \le \alpha \le \pi$ between the outgoing channels in radian units (solid line); the best fit of turning underestimation (dashed line), i.e. $\lambda = 0.87$ in Eq. (15), and for the leaky integrator (dash–dotted line), $\tau_{\mathrm{L}} = 90$ s in Eqs. (19) and (20). The same model errors are applied to a Z–shaped channel and shown in the three lower curves with the same coding (solid, dashed, dotted). Note that errors are smaller, but deviations cancel only partially.

Nonlinear underestimation of the angular turning rate, Eqs. (16) and (17), does not show any different behaviour from (15), because we can assume a *constant* turning rate $\omega_{\mathrm{turn}} = v/r_{\mathrm{turn}} = 4\ \mathrm{s}^{-1}$ given by the ratio of the walking speed $v = 0.2$ m/s and radius of the turn in the channel $r_{\mathrm{turn}} = 0.05$ m, which is half the wall to wall distance, because in experiments deserts ants tend to keep equal distance to both channel walls (T. Merkle, personal observation). However, nonlinear underestimation will lead to different results for arbitrarily curved paths as we will see next.

To investigate how well the different types of systematic errors fit random outbound paths we simulated runs, as they might be performed by an untrained ant searching for food without any knowledge on food sources (see Fig. 8, upper panel). In particular, we considered a fluctuating turning rate $\omega(t)$ with a persistence time T_ω as in Eq. (12) of the model in Section 3.2. For 1000 such runs we extracted correlations between characteristic indicators of the path, such as its integrated curvature $\phi_{\mathrm{end}} - \phi_0 = \int \omega(t)\,dt$, and the two most direct measures for homing deviation: the *angular misestimation* ε between calculated and correct homeward course, and the *euclidean distance* Δ between supposed and real nest positions.

The results are shown in Fig. 6. There is a clear correlation between curvature $\int \omega$ and the directional mismatch of the homing vector, for all error mechanisms except for perception delay (see left panels in column). In particular, all mechanisms tend to *overcompensate* turns effectuated during the outbound path, as there is a *positive correlation* between $\int \omega$ and the deviation angle. Remind that all predict overcompensation for the two–leg experiment of Müller and Wehner as well.

There is a striking difference between the leaky path integrator and the approximative integration formula of Müller and Wehner on one side, and

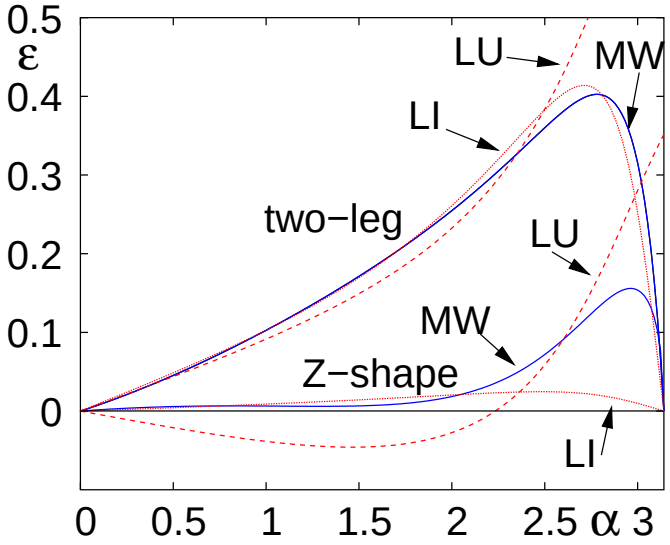

Figure 5: Error angles ε as a function of the intermediate turning angle in the two–leg experiment (three upper curves) and a Z–shaped channel with three parts of 5 m length each (three lower curves) in radian units. Solid lines (MW): Deviation following Müller and Wehner (1988); dashed (LU): linear underestimation of turning rate with $\lambda = 0.87$; dotted (LI): leaky integrator with $\tau_{\mathrm{L}} = 90$ s (resp. $\xi_{\mathrm{L}} = 18$ m). Linear underestimation cannot account for correct path integration under full turns ($\alpha = \pi$) but does well for $0 \leq \alpha \leq (5/6)\,\pi$. In the Z–shaped channel errors are smaller than for single turn and experimentally visible (if at all) only for angles around 150° ($= 5\pi/6$) with errors MW and LU.

turning rate underestimation on the other side: The first two predict a larger euclidean distance from the nest for paths where left and right turns compensate ($\int \omega \approx 0$) and come closer to the nest when there is a substantial net turn, resulting in $\wedge$–shapes in the right hand panels of rows 1 and 2 in Fig. 6. On the other hand, turning rate underestimation predicts smaller distance to the nest for compensated turns, and larger euclidean mismatch for paths with higher turns, leading to $\vee$–shapes of lines 3 and 4 in the right hand panels. Experiments which cover both the *full return path* and the *systematic search*, additionally to the initial direction analysed by Müller and Wehner (1988) may be able to decide the type of homing error mechanism in desert ants (T. Merkle, in preparation).

Fig. 7 shows the homing errors produced by different error types as functions of the distances d between start and end points of foraging trips that had the same overall path lengths. Thus, the values of d indicate the sinuousity of the different paths: straight paths have large, winded paths small d. Roughly speaking the error of the *leaky integrator* increases with d and becomes maximal for perfectly straight paths. The error postulated by Müller and Wehner (1988) also increases with d over a wide range, but *decreases* for very large values for almost straight paths. *Angle underestimation* yields an opposite picture, the deviation decreases over the entire range of d, although large fluctuations may obfuscate measurements. Clearly these findings have to be further developed in comparison to real experiments, but

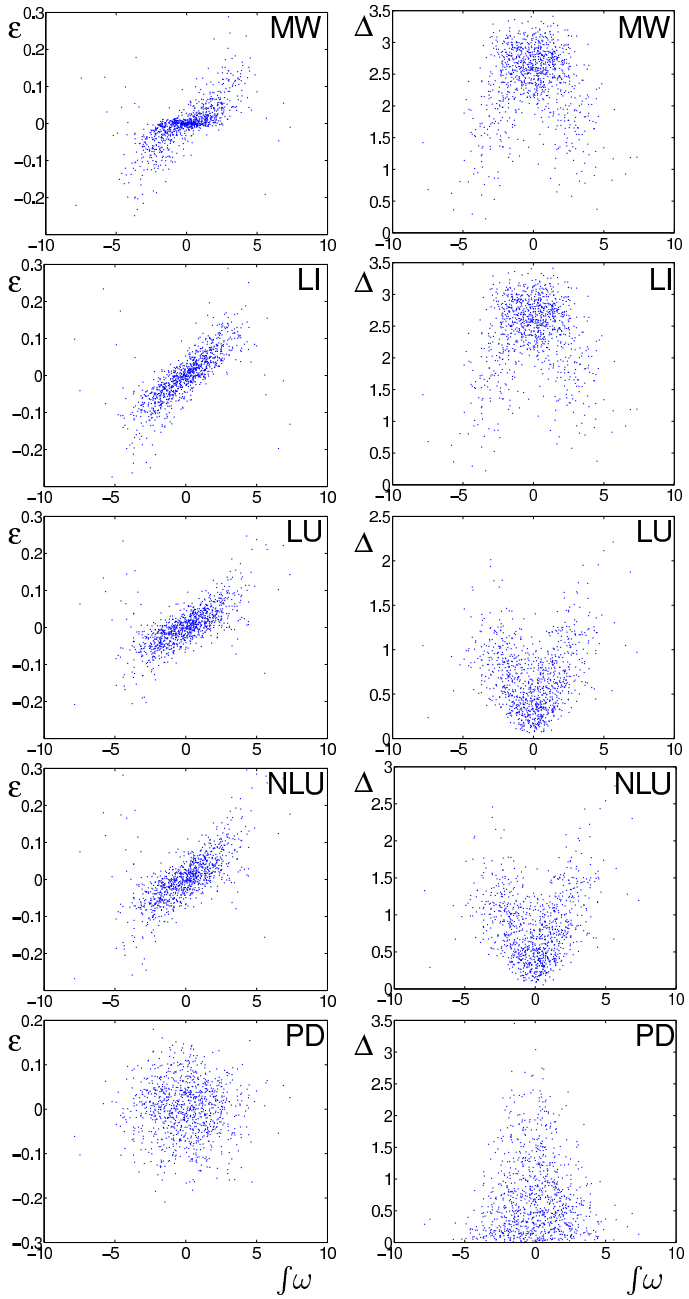

Figure 6: Homing error for different path integration error types as function of integrated curvature $\int \omega(t)\, dt = \phi_{\text{end}} - \phi_0$ (in radians, 2π for full turn) of 1000 simulated random outbound runs of length 20 m each. (Left columns): angular deviation ε in radians; (right columns): euclidean distance Δ from nest in metres. (Top row, MW): error of Müller and Wehner (1988); (2nd row, LI): leaky integrator with $\tau_{\text{L}} = 300$ s; (3rd row, LU): linear underestimation of $\omega(t)$ with $\lambda = 0.87$; (4th row, NLU): nonlinear underestimation; (bottom row, PD): perception delay with $\tau_{\text{del}} = 0.3$ s exhibits no systematic dependence on curvature.

they indicate how field work can enable an observer to differentiate between various error types.

A difference is also visible in the predictions for the supposed nest posi-

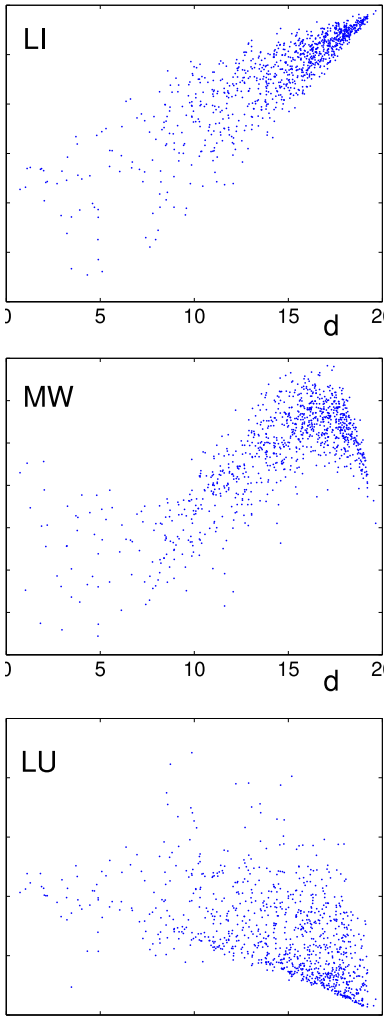

Figure 7: Homing error in euclidean distance Δ between supposed and real nest position as function of distance between starting and end point of foraging path, i.e. distance of feeding site from nest, $0 \leq d \equiv |\boldsymbol{P}(t_1) - \boldsymbol{P}x(0)| \leq 20$. Simulated paths had arch length 20 m, so $d = 20$ m means a perfectly straight path. (Top): The *leaky integrator* predicts increasing Δ with d, whereas according to Müller and Wehner (1988) Δ has a maximum for intermediate d (middle). (Bottom): *Angle underestimation* leads to an opposite relation, Δ decreasing with d. Same parameters as in Fig. 6.

tions, as presented in Fig. 8. In its upper panel it shows the endpoints of two random outbound runs of length 20 m (one in black, the other one in light grey), together with the respective supposed nest locations under different error mechanisms: the formula of Müller and Wehner (MW, marked by $+$), linear (LU, $\Box$) and nonlinear (NLU, $\diamond$) underestimation with $\lambda = 0.87$ and $\omega_c = 0.2$ s^{-1} and turning perception delay with $\tau_{del} = 0.3$ s (PD, $\triangle$). The time constant for the leaky integrator (LI, $\times$), $\tau_L = 300$ s, was chosen such that it best fitted the results of the phenomenological error formula of (Müller and Wehner, 1988). In the lower panel of Fig. 8 the same is shown for 100 paths (without the paths themselves), where all runs start in the same initial direction $\phi_0 = 0$, such that the end points ($\circ$) lie in a sickle

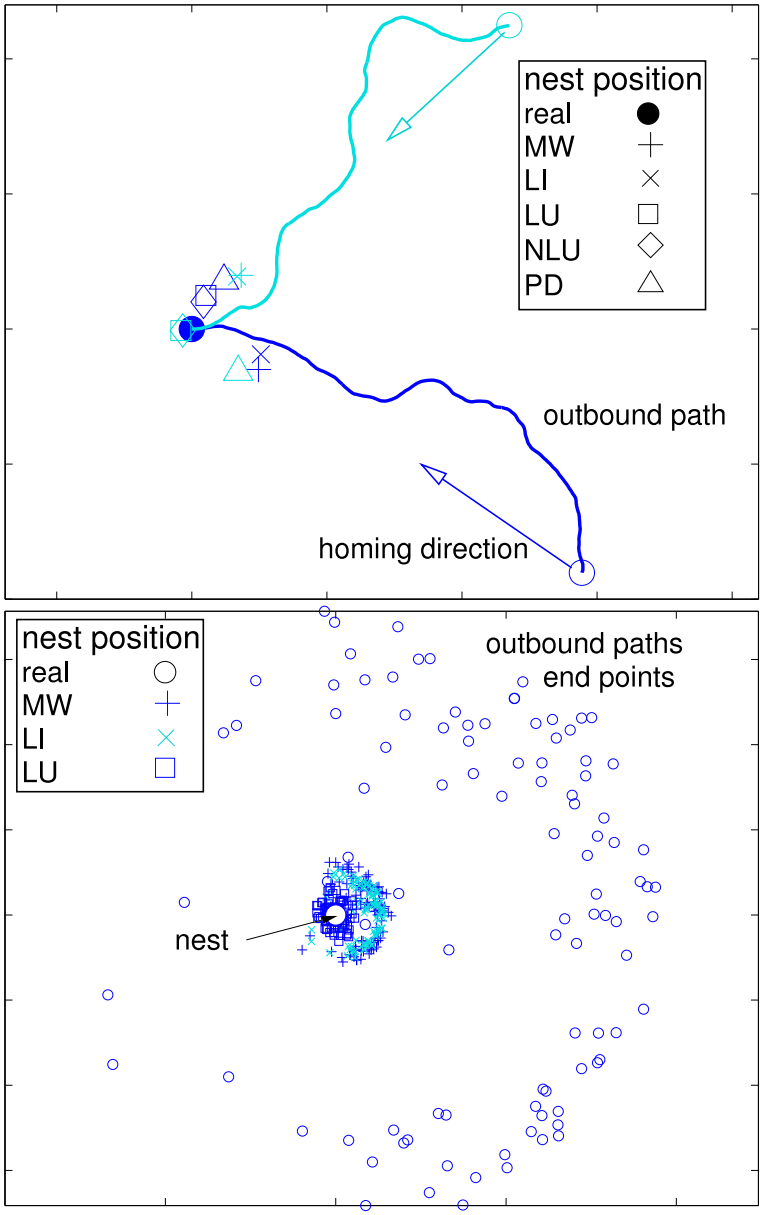

Figure 8: Supposed nest locations for different error types. (Upper panel): Two simulated random outbound paths both starting in direction $\phi_0 = 0$ and having arch length 20 m (black and grey) with supposed nest locations according to Müller and Wehner (+), leaky integrator with $\tau_L = 300$ s (×), underestimation of ω with $\lambda = 0.87$ and $\omega_c = 0.2$ s^{-1} (linear: □, nonlin.: ◇) and processing delay of ω with $\tau_{del} = 0.3$ s (△). Note that (+) and (×) are relatively close. (Lower panel): End points of 100 simulated outbound paths (○) with supposed nest positions after Müller and Wehner (+), leaky integrator (grey ×), and ω–underestimation (□). Real nest marked by filled white circle. Note that (+) and (×) coincide well, in front of real nest. (□) are grouped closely around the nest. Units are in metres.

shaped domain to the right. Again there is a striking coincidence between the leaky integrator and Müller's formula as opposed to the results of turning rate underestimation. Notice that only the two first error mechanisms lead

to a home vector pointing to a location *in front of* the actual nest (see small sickle–shape domain to the right of nest position).

5 Discussion

In this work we have presented a very simple model for path integration using egocentric cartesian coordinates. In contrast to all previous models, including the egocentric one using polar coordinates (Section 2.2), in this model the arthropod does not need to perform complicated calculations such as applying trigonometric or other non–linear functions, but rather updates two cartesian coordinate values of the relative global vector $\boldsymbol{G} = (X, Y)$ by computing a simple system of linear differential equations. Moreover, although we assume that neither the actual relative angle δ nor the distance r to the nest have to be calculated or stored at any time, solely by using the internal $\boldsymbol{G}$–vector information the arthropod has the ability to orient towards the nest position at any time along its path and to hold this orientation during the home run. Keeping $Y = 0$ serves as an 'internal beacon' for home orientation, where the simple counter–steering mechanism can be realized as an elementary negative feedback control of the turning rate by the internal variable Y, until the second internal variable X reaches the desired zero value. Thus, the path integration values (X, Y) do not only provide a record of the arthropod's positional movement, but can also be used as information input for orientation. Moreover, accumulated information on the whole internal (X, Y)-path, as depicted in Fig. 2, for example, may be used by the arthropod to guide its observed systematic search for the 'true' nest position after failure. This could be done by estimating the probability of how far away the nest is located, depending on the probability of the accumulated path integration error. For previous experiments and theories see Hoffmann (1990).

In order to prepare the theoretical background for further investigations, we have restricted this first presentation to (i) construct our model, (ii) implement various error mechanisms and (iii) evaluate their predictions for future comparison with experiments by stochastic simulations. Figs. 6 and 7 suggest simple checks to accept or exclude one or another error mechanism and therefore can serve as a guide for future experiments and modelling.

The mechanisms suggested here could also be tested in experiments with specially designed channels for outbound runs. Different types of angle misestimation would e.g. lead to different systematic deviations of the home run in a channel where left turns are sharper than right turns. Differences between the leaky integrator and angle–misestimation should become apparent in a comparison between two different two–leg experiments, e.g. both with $\alpha = \pi/2$, but two different values $a_1 \neq a_2$ which both would be substantially larger than b.

Physiological realizations of the integration procedure itself and the underlying fundamental neural mechanisms are far from being clarified. Besides, a clarification of the neural processes working in the brain and the locomotory control apparatus of desert arthropods does not seem to be within reach in the near future. We share this problem with all other existing models

of path integration.

On the other hand, anatomic features of neurons, their interactions, their integration, and their cooperation within networks have been known for a long time. Hartmann and Wehner (1995) have developed a simple and efficient neural network for path integration in desert ants. In a particular form it even incorporates the systematic errors observed by Müller and Wehner (1988) on a neural level. Based on their model of an incremental encoding one could easily construct a neural architecture for path integration in cartesian variables X and Y as in Eqs. (9) and (10), where the required estimation of speeds could most likely be encoded by spike rates of afferent neurons.

A further, much simpler way would be to represent the internal cartesian coordinates (X, Y) directly by the deviations of two non–spiking interneuron activities N^X and N^Y from their basal activity values N_0^X and N_0^Y supposed to be attained when the animal is 'at home', i.e. for $(X, Y) = (0, 0)$. Regulation of these interneurons as well as their mutual interactions could then be realized by suitably defined dendritic synapses of a neural net akin to the scheme presented in Fig. 3. Again, the obvious simplicity of this 'linear' control network may favour the egocentric cartesian path integration model as candidate for a most elementary neural realization in the arthropod, compared to other, more complicated models. Although mathematical simplicity is not an ad–hoc argument to explain natural evolution of biological control systems, it is tempting to "grow", i.e. let develop by evolutionary algorithms, neural networks for the task of orientation and analyse their mathematical structure post–hoc, as it has been done for robot motion control (Pasemann et al., 2001).

The ability to find successful feeding sites, also observed for beetles, for instance (von Frisch, 1965), was particularly investigated in detail for desert ants (Wehner et al., 1983; Wehner, 1987; Collett et al., 1999). It is therefore a natural question to ask, whether a similar simple rule as that of keeping $Y = 0$ may help to find a previously known feeding site. Consider all trajectories in geocentric coordinates which keep the egocentric $Y \equiv 0$ constant: they are the radii around the nest position. On the way home they all *converge*, and if by random fluctuations the animal switches over to a trajectory in its neighbourhood it nevertheless is guided towards the nest by the beacon condition $Y = 0$. But for outbound routes they *diverge*, and random errors are not corrected on their own. It would even be better to follow a *fixed compass direction*, because trajectories of the same direction are parallel to each other, and randomly accumulated errors will not be enhanced during the course. In the light of our model it seems natural to suggest that the relative position of a feeding site is internally stored as another global vector $\boldsymbol{G}_\mathrm{f} = (X_\mathrm{f}, Y_\mathrm{f})$ which is updated simultaneously with (X, Y). Depending on whether the animal steers towards the feeder or home, either $Y_\mathrm{f} = 0$ with $X_\mathrm{f} > 0$ is the beacon condition, or $Y = 0$ with $X > 0$. To our knowledge no experiments with obstacles on the way to a trained feeder have been performed corresponding to those described in Wehner (2003) for homing paths with obstacles (see Fig. 2B therein). If the animals are able to compensate forced deviations on the path to the feeder in the same manner as on paths leading home, this would indicate a similar internal processing for both positions.

Moreover, a better understanding of mechanisms by which global vector information is combined or substituted with local information from landmarks requires efficient mathematical models and simulations that are able to reproduce experimental data. With our egocentric path information system for the two relative cartesian coordinates we have presented a most simple modelling tool that can help to evaluate and discriminate various hypotheses on orientation, random or systematic errors, and possible neural representations.

Acknowledgements

This work was partly supported by Research Group *Wissensformate* of Bonn University and Special Research Program SFB 611 of Deutsche Forschungsgemeinschaft. We thank G. Hoffmann for helpful comments on the manuscript, the anonymous referees for many detailed suggestions to improve the manuscript, and R. Wehner for introducing T.M. to *Cataglyphis* and including him in his research project on path integration in desert ants.

References

Alt, W., 1990. Correlation analysis of two-dimensional locomotion paths. In: Alt, W., Hoffmann, G. (Eds.), Biological Motion. Lecture Notes in Biomathematics Vol 89. Springer, Berlin, Heidelberg and New York, pp. 154–168.

Alt, W., 1995. Elements of a systematic search in animal behavior and model simulations. Bio Systems 34, 11–26.

Benhamou, S., 1996. No evidence for cognitive mapping in rats. Anim. Behav. 52, 201–212.

Benhamou, S., 1997. Path integration by swimming rats. Anim. Behav. 54, 321–327.

Benhamou, S., Sauve, P., Bovet, P., 1990. Spatial memory in large scale movements: efficiency and limitation of the egocentric coding process. J. Theor. Biol. 145, 1–12.

Benhamou, S., Séguinot, V., 1995. How to Find one's Way in the Labyrinth of Path Integration Models. J. Theor. Biol. 174, 463–466.

Biegler, R., 2000. Possible uses of path integration in animal navigation. Anim. Learn. Behav. 28, 257–277.

Bisch, S., 1999. Orientierungsleistungen des nachtaktiven Wüstenkäfers *Parastizopus armaticeps* Peringuey (Coleoptera: Tenebrionidae). Dissertation. Bonn.

Bisch-Knaden, S., Wehner, R., 2003. Local vectors in desert ants: context-dependent landmark learning during outbound and homebound runs. J. Comp. Physiol. A 189, 181–187.

Bisetzky, A. R., 1957. Die Tänze der Bienen nach einem Fussweg zum Futterplatz. Z. Vergl. Physiol. 40, 264–288.

Byers, J. A., 2001. Correlated random walk equations of animal dispersal resolved by simulation. Ecology 82, 1680–1690.

Collett, M., Collett, T. S., Bisch, S., Wehner, R., 1998. Local and global vectors in desert ant navigation. Nature 394, 269–272.

Collett, M., Collett, T. S., Chameron, S., Wehner, R., 2003. Do familiar landmarks reset the global path integration of desert ants? J. Exp. Biol. 206, 877–882.

Collett, M., Collett, T. S., Wehner, R., 1999. Calibration of vector navigation in desert ants. Curr. Biol. 9, 1031–1034.

Darwin, C., 1873. Origin of certain instincts. Nature 7, 417–418.

Dyer, F. C., Dickinson, J. A., 1994. Development of sun compensation by honeybees: how partially experienced bees estimate the sun's course. Proc. Natl. Acad. Sci. 91, 4471–4474.

Eggers, A., Gewecke, M., 1993. The dorsal rim area of the compound eye and polarization vision in the desert locust *Schistocerca gregaria*. In: Wiese, K., Gribakin, F. G., Popov, A. V., Renninger, G. (Eds.), Sensory systems of arthropods. Birkhäuser; Basel, Boston and Berlin, pp. 101–109.

Etienne, A. S., Jeffry, K. J., 2004. Path integration in mammals. Hippocampus 14, 180–192.

Etienne, A. S., Maurer, R., Séguinot, V., 1996. Path integration in mammals and its interaction with visual landmarks. J. Exp. Biol. 199, 201–209.

Fent, K., 1986. Polarized skylight orientation in the desert ant *Cataglyphis*. J. Comp. Physiol. A 185, 145–150.

Frisch, K. v., 1949. Die Polarisation des Himmelslichts als orientierender Faktor bei den Tänzen der Bienen. Experientia 5, 142–148.

Frisch, K. v., 1950. Die Sonne als Kompaß im Leben der Bienen. Experientia 6, 210–222.

Frisch, K. v., 1965. Tanzsprache und Orientierung der Bienen. Springer; Berlin, Heidelberg and New York.

Gallistel, C. R., 1990. The Organization of Learning. Cambridge, MA.: Bradford books/MIT press.

Görner, P., 1958. Die optische und kinästhetische Orientierung der Trichterspinne *Agelena labyrinthica* (Cl.). Z. Vergl. Physiol. 41, 111–153.

Görner, P., 1966. Über die Koppelung der optischen und kinästhetischen Orientierung bei der Trichterspinne *Agelena labyrinthica* (Cl.) und *Agelena gracilens* (C.L. Koch). Z. Vergl. Physiol. 53, 252–276.

Hartmann, G., Wehner, R., 1995. The ant's path integration system: a neural architecture. Biol. Cybern. 73, 483–497.

Hoffmann, G., 1984. Orientation behaviour of the desert woodlouse *Hemilepistus reaumuri*: adaptions to ecological and physiological problems. In: Sutton, S. L., Holdich, D. M. (Eds.), The biology of terrestrial isopods. Symp Zool Soc; London, pp. 405–422.

Hoffmann, G., 1985a. The influence of landmarks on the systematic search behaviour of the desert isopod *Hemilepistus reaumuri*. I. Role of the landmark made by the animal. Behav. Ecol. Sociobiol. 17, 325–334.

Hoffmann, G., 1985b. The influence of landmarks on the systematic search behaviour of the desert isopod *Hemilepistus reaumuri*. II. Problems with similar landmarks and their solutions. Behav. Ecol. Sociobiol. 17, 335–348.

Hoffmann, G., 1990. The site independent information that an isopod uses for homing. In: Alt, W., Hoffmann, G. (Eds.), Biological Motion. Lecture Notes in Biomathematics Vol 89. Springer, Berlin, Heidelberg and New York, pp. 305–318.

Itô, K., McKean, P., 1965. Diffusion Processes and Their Sample Paths. Springer; Berlin, Heidelberg and New York.

Jander, R., 1957. Die optische Richtungsorientierung der Roten Waldameise (*Formica rufa*). Z. Vergl. Physiol. 40, 162–238.

Jander, R., 1970. Ein Ansatz zur modernen Elementarbeschreibung der Orientierungshandlung. Z. Tierpsychol. 27, 771–778.

Keil, T. A., 1997. Functional Morphology of Insect Mechanoreceptors. Microsc. Res. Tech. 39, 506–531.

Maurer, R., Séguinot, V., 1995. What is modelling for? A critical review of the models of path integration. J. Theor. Biol. 175, 457–475.

Mittelstaedt, H., 2000. Triple-loop model of path control by head direction and place cells. Biol. Cybern. 83, 261–270.

Mittelstaedt, H., Mittelstaedt, M. L., 1973. Mechanismen der Orientierung ohne richtende Aussenreize. Fortschr. Zool. 21, 46–58.

Mittelstaedt, H., Mittelstaedt, M. L., 1982. Homing by path integration. In: Papi, F., Wallraff, H. G. (Eds.), Avian Navigation. Springer; Berlin, Heidelberg and New York, pp. 290–297.

Mittelstaedt, M. L., Mittelstaedt, H., 1980. Homing by path integration in a mammal. Naturwiss. 67, 566.

Mittelstaedt, M. L., Mittelstaedt, H., 2001. Idiothetic navigation in humans: estimation of path length. Exp. Brain. Res. 139, 318–332.

Müller, M., Wehner, R., 1988. Path integration in desert ants, *Cataglyphis fortis*. Proc. Natl. Acad. Sci. USA 85, 5287–5290.

Pasemann, F., U. Steinmetz, U., Hülse, M., Lara, B., 2001. Robot control and the evolution of modular neurodynamics. Theory in Biosciences 120, 311–326.

Ronacher, B., Wehner, R., 1995. Desert ants *Cataglyphis fortis* use self-induced optic flow to measure distances travelled. J. Comp. Physiol. A 177, 21–27.

Rossell, S., Wehner, R., 1984. Celestial orientation in bees: the use of spectral cues. J. Comp. Physiol. A 155, 605–613.

Samsonovich, A., McNaughton, B. L., 1997. Path Integration and Cognitive Mapping in a Continuous Attractor Neural Network Model. J. Neurosci. 17, 599–5920.

Schäfer, M., Wehner, R., 1993. Loading does not affect measurement of walking distance in desert ants, *Cataglyphis fortis*. Verh. Dt. Zool. Ges. 86, 270.

Séguinot, V., Cattet, J., Benhamnou, S., 1998. Path integration in dogs. Anim. Behav. 55, 787–797.

Séguinot, V., Cattet, J., Etienne, A. S., 1993. Dead reckoning in a small mammal: the evaluation of distance. J. Comp. Physiol. A 173, 103–113.

Sommer, S., Wehner, R., 2004. The ant's estimation of distance travelled: experiments with desert ants, *Cataglyphis fortis*. J. Comp. Physiol. A 190, 1–6.

Wehner, R., 1968. Optische Orientierungsmechanismen im Heimkehrverhalten von *Cataglyphis bicolor* (Formicidae, Hymenoptera). Rev. Suisse Zool. 75, 1076–1085.

Wehner, R., 1987. Spatial organization of foraging behavior of individually searching desert ants, *Cataglyphis* (Sahara desert) and *Ocymyrmex* (Namib desert). In: Pasteels, J. M., Deneubourg, J. L. (Eds.), From individual to collective behavior in social insects. Birkhäuser; Basel and Boston, pp. 15–42.

Wehner, R., 1994. The polarization-vision project: championing organismic biology. Fortschr. Zool. 39, 103–143.

Wehner, R., 1997a. The ant's celestial compass system: spectral and polarization channels. In: Pasteels, J. M., Deneubourg, J. L. (Eds.), Orientation and Communication in Arthropods. Birkhäuser; Basel, pp. 145–185.

Wehner, R., 1997b. Insect navigation: low-level solutions to high-level tasks. In: Srinivasan, M. V., Venkatesh, S. (Eds.), From Living Eyes to Seeing Machines. Oxford University Press; New York, pp. 158–173.

Wehner, R., 1998. Der Himmelskompaß der Wüstenameisen. Spektrum der Wissenschaft 11, 56–67.

Wehner, R., 2001. Polarization vision - a uniform sensory capacity? J. Exp. Biol. 204, 2589–2596.

Wehner, R., 2003. Desert ant navigation: how miniature brains solve complex tasks. Karl von Frisch Lecture. J. Comp. Physiol. A 189, 579–588.

Wehner, R., Harkness, R. D., Schmid-Hempel, P., 1983. Foraging Strategies of Individually Searching Ants *Cataglyohis bicolor*. Gustav Fischer Verlag; Stuttgart and New York.

Wehner, R., Michel, B., Antonsen, P., 1996. Visual navigation in insects: coupling of egocentric and geocentric information. J. Exp. Biol. 199, 129–140.

Wehner, R., Müller, M., 1993. How do ants acquire their celestial ephemeris function. Naturwiss. 80, 331–333.

Wehner, R., Srinivasan, M. V., 2003. Path integration in insects. In: Jeffery, K. J. (Ed.), The neurobiology of spatial behaviour. Oxford University Press; Oxford, pp. 9–30.

Wehner, R., Wehner, S., 1986. Path integration in desert ants: approaching a long-standing puzzle in insect navigation. Monit. Zool. Ital. 20, 309–331.

Wohlgemuth, S., Ronacher, B., Wehner, R., 2002. Distance estimation in the third dimension in desert ants. J. Comp. Physiol. A 188, 273–281.

Ziegler, P. E., Wehner, R., 1997. Time-courses of memory decay in vector-based and landmark-based systems of navigation in desert ants, *Cataglyphis fortis*. J. Comp. Physiol. A 181, 13–20.